We are IntechOpen, the world's leading publisher of Open Access books Built by scientists, for scientists

4,800
Open access books available

122,000
International authors and editors

135M
Downloads

Our authors are among the

154
Countries delivered to

TOP 1%
most cited scientists

12.2%
Contributors from top 500 universities

CLARIVATE ANALYTICS BOOK CITATION INDEX INDEXED

WEB OF SCIENCE™

Selection of our books indexed in the Book Citation Index in Web of Science™ Core Collection (BKCI)

Interested in publishing with us?
Contact book.department@intechopen.com

Numbers displayed above are based on latest data collected.
For more information visit www.intechopen.com

9

Geiger-Mode Avalanche Photodiodes in Standard CMOS Technologies

Anna Vilà, Anna Arbat, Eva Vilella and Angel Dieguez
Electronics Department, University of Barcelona
Spain

1. Introduction

Photodiodes are the simplest but most versatile semiconductor optoelectronic devices. They can be used for direct detection of light, of soft X and gamma rays, and of particles such as electrons or neutrons. For many years, the sensors of choice for most research and industrial applications needing photon counting or timing have been vacuum-based devices such as Photo-Multiplier Tubes, PMT, and Micro-Channel Plates, MCP (Renker, 2004). Although these photodetectors provide good sensitivity, noise and timing characteristics, they still suffer from limitations owing to their large power consumption, high operation voltages and sensitivity to magnetic fields, as well as they are still bulky, fragile and expensive. New approaches to high-sensitivity imagers tend to use CCD cameras coupled with either MCP Image Intensifiers, I-CCDs, or Electron Multipliers, EM-CCDs (Dussault & Hoess, 2004), but they still have limited performances in extreme time-resolved measurements.

A fully solid-state solution can improve design flexibility, cost, miniaturization, integration density, reliability and signal processing capabilities in photodetectors. In particular, Single-Photon Avalanche Diodes, SPADs, fabricated by conventional planar technology on silicon can be used as particle (Stapels et al., 2007) and photon (Ghioni et al., 2007) detectors with high intrinsic gain and speed. These SPAD are silicon Avalanche PhotoDiodes biased above breakdown. This operation regime, known as Geiger mode, gives excellent single-photon sensitivity thanks to the avalanche caused by impact ionization of the photogenerated carriers (Cova et al., 1996). The number of carriers generated as a result of the absorption of a single photon determines the optical gain of the device, which in the case of SPADs may be virtually infinite.

The basic concepts concerning the behaviour of G-APDs and the physical processes taking place during their operation will be reviewed next, as well as the main performance parameters and noise sources.

1.1 Basic concepts for Geiger-mode avalanche photodiodes, G-APDs

APDs can be obtained by implementing two possible approximations that produce two different structures with differentiated capabilities. On one hand, thin silicon APDs (Lacaita et al., 1989) are devices with a depletion layer of few micrometres and low breakdown voltages. They also present good detection efficiency and time resolution. As in planar

APDs it is important to avoid the possibility of edge breakdown of the sensor, many different terminations have been proposed, generating a variety of planar CMOS compatible devices. On the other hand, thick APDs (Cova et al., 2004) are devices with a depletion layer of some tens of micrometres that work at high breakdown voltage; they have good detection efficiency but moderate time resolution. These components are fabricated in dedicated technologies, increasing their cost.

An example of these two different structures is shown in Fig. 1.A: a thick APD at the left side (Alexander, 1997) and a thin APD at the right side. The structures are composed of different sections of semiconductor with different doping profiles shown in B. In C, the charge density of the structures is represented. The p region develops a net negative charge, while the n region develops a net positive charge, generating the energy diagrams visible in D and an electric field profile such as in E.

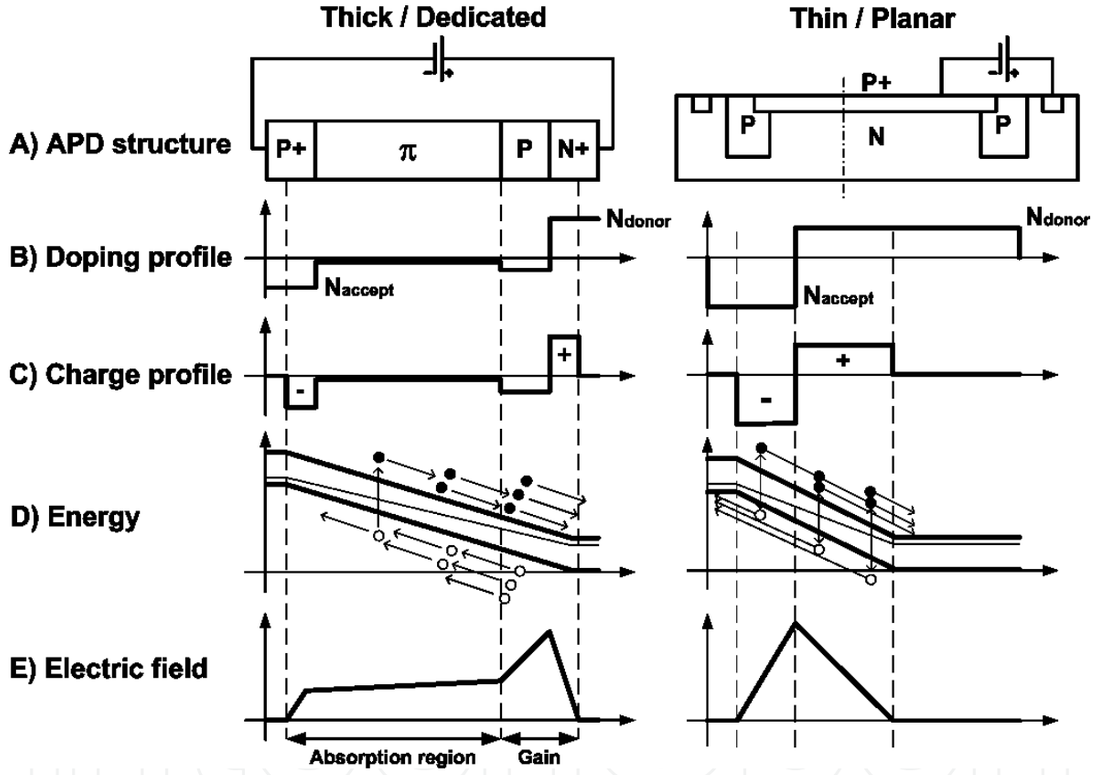

Fig. 1. Comparison between thick (left) and thin (right) APD structures. A) structure, B) doping profile across the dash-dotted line in A, C) charge profile, D) energy-band diagram, E) electric field profile.

An electron-hole pair, EHP, can be generated due to photon absorption, minimum-ionizing particle crossing the detector or by thermal generation. Due to the electric field in the sensing area, carriers are accelerated to the collection zone. The high electric field give to the carriers enough kinetic energy to produce additional EHP by impact ionization. This additional charge is also accelerated and eventually produces new EHP in their way towards the electrodes. The whole effect generates a multiplication of the electric signal from a single photon.

There are two possible operation modes depending on the biasing of the APD: linear (Fig. 2.A) and Geiger (Fig. 2.B). In the linear mode, only the electrons achieve enough kinetic energy to produce new EHPs by impact ionization, producing gains around 1000 (Kindt, 1994). The gain is then moderate and affected by strong excess noise (McIntyre, 1972), making difficult the detection of single photons. The gain is strongly dependent on the biasing voltage, requiring a uniform field over the sensible area to have a constant gain. When the device is biased well above the breakdown voltage, Geiger mode, the electric field in the depletion layer is so high that also holes produce new EHPs, generating a self-sustaining avalanche current. In this case, the avalanche can be triggered by a single photon or a single EHP generated by a MIP, and the device becomes a SPAD. The current rises swiftly (sub-nanosecond rise-time) to a macroscopic steady level in the milliampere range, irrespective to the quantity of photons detected (essential effect for silicon photomultipliers, where the output signal is proportional to the number of APDs in avalanche).

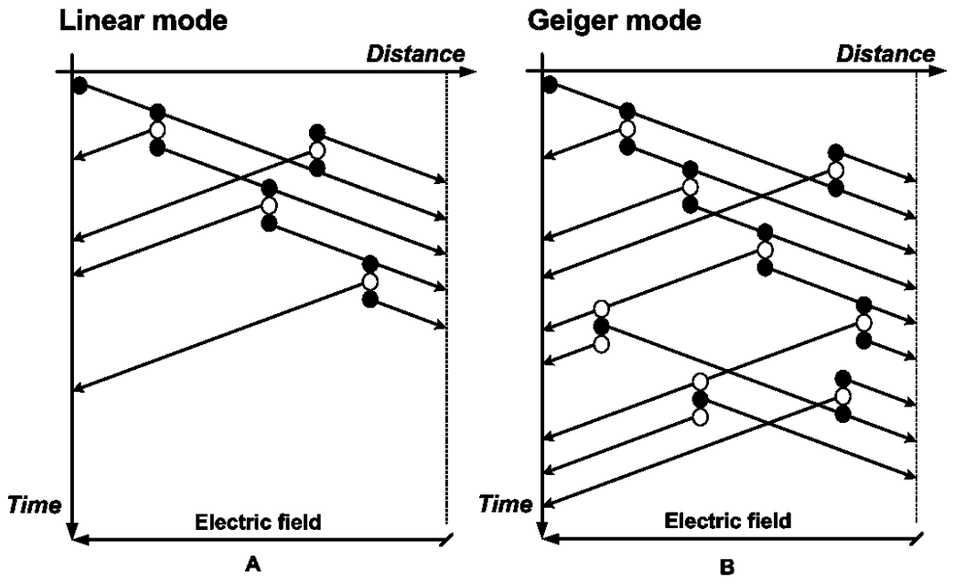

Fig. 2. Avalanche phenomena due to impact ionization. A) In linear mode, only electrons contribute to EHP generation. B) In Geiger mode, both electrons and holes produce newEHPs, promoting a self-sustained avalanche.

In Geiger mode, the current generated during the avalanche continues to flow until lowering the bias voltage down to the breakdown quenches it. Then, the lower electric field is no longer able to accelerate carriers to impact-ionize lattice atoms, therefore current ceases. In order to be able to detect another photon, the biasing needs to be restored to the initial value in a recharge process to leave the detector ready to work again.

Consequently, the detection cycle includes the quenching and the recharge periods, and usually specific circuitry helps to do these actions. The basic goal is to limit the avalanche charge flowing through the APD at every ignition, in order to reduce three detrimental effects:

- Afterpulsing: avalanche events produced by the release of charges trapped into deep levels (Cova et al., 1996).

- Self-heating: more dark counts are generated, but also breakdown voltage is increased and excess voltage decreased, reducing the detection efficiency.
- Crosstalk: interference between neighbouring sensors produced by emission of secondary photons (Zappa et al., 1997).

1.1.1 Performance parameters

In this context, the main figures of merit that have been used to describe the capabilities of G-APDs as photodetectors are shortly reviewed next. Some of them are specific of the case under study and have no sense related to other types of technologies. However, all they are of crucial importance in G-APDs.

Gain

First of all, the gain or multiplication factor, M, is defined as the ratio between the observable photocurrent at the APD terminals and the internal photocurrent before multiplication. This primary photocurrent depends on the detector quantum efficiency, defined as the number of electrons collected in a pixel over the number of photons penetrating it, the photon energy and the received optical signal power. This effect is similar to that achieved with a photomultiplier.

Ionization coefficients

The ionization coefficients for electrons and holes, α_e and α_h respectively, are defined as the probability that the carrier causes some ionization within a unit length. These coefficients increase with the field, as the carrier achieves a higher energy, while decreases with temperature, as the atoms are thermally excited, reducing the collision probability. High-quality APDs can present a ratio between α_h and α_e of between 0.003 and 0.01.

Time delay

The time delay of an avalanche corresponds to the time between the photodiode generates an EHP and the avalanche arrives to the measuring circuit, and it represents a fundamental parameter of an APD because it, together with the RC time-constant and the transit time, determines its bandwith. The time delay is determined by the transition times for the electrons/holes to reach the avalanche region (i.e. the time required for charges to go through an absorption region and arrive to the avalanche region) and the avalanche build-up time.

Timing resolution or jitter

The timing resolution or timing jitter of the sensor is defined as the statistical fluctuation of the time interval between the arrival of the photons at the sensor and the output-pulse leading edge. It can be described as the full-width half-maximum measure of the temporal variation in the avalanche breakdown pulses resulting from an incident photon beam. Among the timing-resolution components are the variation caused by the generated-carrier transit time from the depletion layer to the multiplication region, which is dependent on the depth of absorption of the incident photon and, more important, the statistical build up of the avalanche current itself (Ghioni et al., 1988), which timing improves with the excess bias voltage.

Photon detection efficiency, PDE, or photon detection probability, PDP

The photon detection efficiency, PDE, is the probability of avalanche generation for each detected photon. For a photon to be detected, it must be absorbed in the detector active volume and generate a primary carrier, but it is also necessary for this primary carrier to succeed in triggering an avalanche. The photon detection probability, PDP, is related to the PDE, and it is defined as the probability of a photon to generate an avalanche. Both concepts are wavelength dependent and increase with the excess bias voltage, as the higher electric field enhances the triggering probability.

Sensitivity or dynamic range

The dynamic range, DR, quantifies the ability of a sensor to adequately image both clear lights and dark shadows in the same scene. It is defined as the maximum signal divided by the noise. In the case of APDs, the DR is given by the maximum number of counts generated by the sensor and the dark count noise. The sensitivity increases with the biasing voltage and depends on the technology.

Fill factor

The fill factor is the ratio between the light-sensitive area of a pixel and its total area. The electric field strength should be consistent across the whole active area (the central photon-sensitive portion of the detector), so as to yield a homogeneous breakdown probability. However, electric field concentration at the edges and corners can cause higher photon-detection probability and dark counts. Such zones should be avoided by proper design solutions such as guard rings or shallow trenches, which limit the active detector volume. This is a main drawback for present G-APDs, especially for large-area high-precision applications such as particle detectors in colliders or telescopes.

Dead time

The dead time is the time during which the sensor is not responsive to further incoming photons, due primarily to accumulation of charge in the active region. It involves the periods comprising the avalanche quenching and the device recharge, i.e. the reset of the final bias conditions. However, in the case of a passively quenched SPAD this is not strictly the case, because, as the device is recharged via the quenching resistor, it becomes increasingly biased beyond its breakdown voltage, so it is able to detect the next photon arrival prior to being fully reset. This behaviour is coupled with a significant fluctuation in the reset waveform and can increase the afterpulsing probability due to inadequate trap flushing time.

1.1.2 Noise sources

The inherent noise sources of APDs are dark counts and afterpulsing events. There is also an external noise source between neighbouring sensors due to electrical and optical crosstalk.

Dark count rate, DCR

A dark count is an avalanche event caused by non-photogenerated carriers, which can be originated from four factors (Haitz, 1965): diffusion from neutral regions, thermal generation, band-to-band tunnelling or by release from a charge trap (see also afterpulsing).

This generation is critical when operating in Geiger mode, as it can produce an output pulse indistinguishable from the one originated by a detection event. The per-second rate at which dark counts occur is the DCR in Hertz.

Dark-count noise increases with temperature, as the thermal carrier generation increases and so the probability of avalanche. It also increases with the excess voltage because of two effects, namely the field-assisted enhancement of the emission rate from generation centres and the increase of the avalanche-triggering probability with the higher electric field at the depletion layer, which reduces the recombination probability. Of course, thermal generation is strongly dependent on the fabrication process, which determines the concentration of traps, the breakdown voltage and the avalanche probability. On the contrary, tunnelling generation depends on the doping profile and the bias voltage, and its temperature dependence is weak.

Afterpulsing

Charge traps due to unintentional impurities and crystal defects can result in generation-recombination centres. The high current peak through the junction during an avalanche breakdown introduces a probability that the trap is filled by a carrier that is later released, initiating a second, follow-on Geiger 'after-pulse' (Haitz, 1965). Afterpulsing is then a false detection caused by secondary dark pulses correlated to a previous primary one. This phenomenon suffers from a statistical fluctuating delay whose mean value depends on the deep levels actually involved.

The number of carriers captured during an avalanche pulse increases with the total number of carriers crossing the junction, that is, with the total charge involved in the avalanche pulse, and with the number of traps in the multiplication area. Therefore, afterpulsing increases with the delay of avalanche quenching and with the current intensity, which is proportional to the excess bias voltage. This overvoltage also enlarges the depletion zone, and so the number of available traps, increasing the trapping probability. Finally, released charges can retrigger avalanche.

Crosstalk

A crosstalk is a signal interference between neighbouring pixels produced by electrical or optical interaction between them. The electrical crosstalk corresponds to the migration of carriers from one pixel to another, and can be probably reduced by a potential barrier designed properly to collect these charges. On the other hand, hot carriers in an avalanche emit 2.9 photons per 10^5 electrons (Lacaita et al., 1993) that can produce an avalanche in the neighbouring pixel generating an optical crosstalk. The probability of this phenomenon depends on many factors, such as pixel size, dead space between active areas, sensitive volume and gain, but it can be diminished by reducing the number of carriers generated in the avalanche.

2. Technology considerations for GAPDs

This section consists on a review of the fundamental technology considerations that deserve to be taken into account referred to the actual G-APDs, including the state-of-the-art of avalanche photodiodes fabricated in CMOS compatible technologies.

2.1 Historical review of APDs technologies

The switching effect observed in reverse-biased silicon p-n junctions by McKay (McKay, 1954), marked the beginning on the study of the structures in avalanche. Imperfect junctions with a large number of impurities were used in initial investigations. In 1961 Shockley (Shockley, 1961) proposed the ideal reverse junction characteristics which were confirmed in the early 1960s (Goetzberg et al., 1963), (Haitz, 1964) and (Haitz, 1965). With initial progresses of silicon technology, it was possible to fabricate better junctions nearly free from defects (called microplasmas by then). But practical devices were large (about 1mm^2) and they did not attract much attention due to their high cost low efficiency.

In the early 70s, McIntyre (McIntyre, 1972) and Webb (Webb et al., 1974) developed new APD structures that were the precursors of commercial devices implemented in the Single Photon Counting Modules, SPCM. These new devices were fabricated on a sophisticate dedicated process which was incompatible with the planar technology (thick-APDs), but improved the photodetection efficiency. This was the beginning of dedicated technologies for APDs, able to reduce the dark count noise and improve the features of the detector.

Evolution has allowed APDs exhibiting excellent quantum efficiency, with values around 80% in the near ultra-violet range, dropping to about 40% in the blue region, which is to be compared to typical values of 5-8 % in the blue for standard photomultipliers. Although in the late 80s the planar technology to fabricate APDs was improved by Ghioni when they introduced the first epitaxial device structure (Ghioni et al., 1988), nowadays mainly all commercial APDs are produced by dedicated technologies not compatible with CMOS planar technology, what increases the difficulty to integrate an array of detectors together with the control electronics.

At the beginning of the XXI century the research on APDs was reoriented to the integration of the sensors together with the electronics thanks to the improvement on the CMOS technologies. Main objectives were the fabrication of SPAD integrated cameras (Charbon, 2007) and of large SPADs, which were restricted to the dedicated technologies (Ghioni et al., 2007). The first APDs in CMOS compatible technologies were published by research centers (Spinelli et al., 1998, Jackson et al., 2001 and Gulinatti et al., 2005). They were developed using the high voltage CMOS, HV-CMOS, technologies (Rochas et al., 2002 and Zappa et al., 2004), as they provide a relatively low-doped deep n-well that allows up to 50 V of isolation from the substrate (Rochas et al., 2003a) and low noise detectors.

The first SPAD-based pixel array in CMOS technology has been demonstrated a few years ago (Rochas et al., 2003b), consisting on a 4 by 8 array of SPADs with a passive quenching circuit and a simple comparator (inverter). Further developments followed quickly, facilitated by the availability of commercial HV-CMOS technologies and of specially tailored imaging processes boosted by the huge market of mobile phone cameras. Designs using a 0.8 μm CMOS technology have also been presented. In (Niclass & Charbon, 2005) a 64x64 image sensor with single pixel readout is employed for 3D imaging. Another APD array based on event-driven reading was also developed using the same technology (Niclass et al., 2006a). The evolution of the technologies also produces an evolution on the sensors, and some arrays were presented using 0.35 μm technology (Sergio et al., 2007). An array of 128x2 APDs was developed including latches to preserve the timing information. Finally the evolution of APDs arrived to 130 nm, with an array of 32x32 sensors (Guerrieri et al., 2009).

In the last years, the use of submicronic technologies has also included the study of APD structures, and some comparison between technologies has been reported recently (Arbat et al., 2010a), concluding that high-voltage technology has a low dark-count rate related to the low trap concentration but the sensor is slow, while high-integration technology generates fast sensors with high dark count rates. In 2006 Finkelstein presented a new structure for an APD based on shallow-trench isolation, STI (Finkelstein et al., 2006a). Although a reduction of size, the structure suffered from many dark counts that limited the device performances. In 2007, an n-well-based structure was designed on a 130nm technology (Niclass et al., 2007a and b), and the modifications needed for the 130nm-process to improve the detector features were presented (Gersbach et al., 2008). With the same 130nm technology, p-guard STI structures were also proposed (Gersbach et al., 2009), as well as a lower p-doping well in a deep n-well (Richardson et al., 2009). Going further, the first APD structures obtained using 90nm technology have been reported (Karami et al., 2010). In a parallel way, the use of nanostructures of germanium deposited in silicon to obtain small APDs able to work at voltages of only 1.5V and speeds of 30GHz have been proposed (Assefa et al., 2010). Even, a novel effort to use APDs to construct detectors for charged particles has recently been reported (Graugés et al., 2010, Vilà et al., 2011). Results suggest that, through control of the doping concentration, devices with a much improved fill factor could be achieved. Consequently, submicron CMOS technologies with ever decreasing minimum feature size seem to be useful for SPAD fabrication.

2.2 Dedicated vs. standard technologies

The present situation of SPADs may be described in terms of the manufacturing processes and construction details. In particular, two main process categories can be distinguished:

a. Dedicated technologies, which improve performances by optimizing individual technological parameters. They generate low-noise high-quantum-efficiency sensors via thick depletion layers (> 30μm), but integration of electronics with sensor is impossible.
b. CMOS compatible technologies, which can be only compatible (i.e. full-custom processes optimized to yield the best possible performing single detector element) or standard CMOS processes, without any modifications to the layers normally available to the designers. Both single detectors and arrays have been implemented with HV-CMOS processes (Rochas et al., 2003a and b, Stoppa et al., 2007 and Vilà et al., 2011), demonstrating their suitability for SPADs.

Both types of APD processes offer different features. In Table 1, a comparative of the main characteristics of each type of sensors is given. As APDs are mainly used as photon detectors, the detection efficiency is given for wavelengths. When high-energy particles are considered, the detection efficiency is related to the number of electrons generated by ionization in the multiplication region due to the crossing particle.

A method to build a thick APD using dedicated technologies consists on building the sensor on a p substrate with an n+ layer on one side and a p+ diffused layer to improve the ohmic contact on the other side (Webb et al. 1974). This produces a reach-through structure formed by four layers in a vertical structure, generating a p+-π-p-n+ stack (see figure 1) that can be improved through processes covered by patents (McIntyre, 1990 and 1996). As its operation is based on the complete depletion of the device (30 to 100μm deep), the required voltages are high, typically over 100V. This produces sensors with low noise and high quantum

efficiency (Cova et al., 2004, Lacaita et al., 1988 and Ghioni & Ripamonti, 1991). This technology allows the possibility to produce wide active areas, up to 500 μm in diameter, with variable depletion-layer thickness (Dautet et al., 1993).

Main features	Planar – Thin	Dedicated - Thick
Breakdown	10 – 50 V	100 – 500 V
Multiplication thickness	1 – 2 μm	30 – 100 μm
Active area diameter	5 – 150 μm	100 – 500 μm
Photon Detection Efficiency (PDE)	~ 45 % @ 500 nm ~ 32 % @ 630 nm ~ 15 % @ 730 nm ~ 10 % @ 830 nm 0.1 % @ 1064 nm	> 50 % @ 540 - 850 nm ~ 3 % @ 1064 nm
Resolution in photon timing	<100 ps FWHM	< 350 ps reach-through ~ 150 ps smoother field profile
Dark count rate	Technology dependent	Very low noise
Power dissipation	Low, cooling system not required	High, cooling system required
Array fabrication	Compatible	Not compatible
Robustness	Good	Delicated
Cost	Low	High

Table 1. Dedicated vs. planar technologies comparison.

There are some commercial compact modules that include the bias and the quenching circuitry (Spinelli et al., 1996 and EG&G, 1996). Some performances of commercial APDs based in reach-through structures are given in Table 2. Although the reach-through structures have good performance, they also have a number of practical drawbacks. The main problem is the high power dissipation due to the high biasing voltage, arriving to values of 5 to 10 W. Another negative aspect is the high fabrication cost of the sensors, due to a low fabrication yield. Finally, the produced devices are delicate and degradable, and of course not integrable with circuitry.

Feature	InGaAs	Si	Array 4x8
Active area (mm)	0.04	0.2 - 5	1.6 x 1.6 Pitch 2.3mm
Wavelength (nm)	950 - 1700	200 - 1100	320 - 1000
λ peak (nm)	1550	620 – 940	600
Sensibility @ λp (A/W)	0.8 – 0.9	0.42 -0.5	-
Quantum efficiency (%)	-	75 - 80	70
V breakdown (V)	40 - 60	150 - 300	400 - 500

Table 2. Hammamatsu commercial APD features.

APD devices developed in planar technologies generate a thin depletion layer of few micrometers, being called thin APDs. These devices are generated by epitaxy over silicon wafers (Spinelli et al., 1998). Over the last years, improvements of the technology to fabricate integrated circuits have allowed the development of APDs integrated in commercial CMOS

Reference	Technolgy (termination)	Diameter (μm)	V_{BD} (V)	DCR (c/s)	PDE (%) @500nm	FWHM (ps)
(Spinelli et al., 1998)	Double junction	10	27	-	35	35
(Jackson et al., 2001) (Jackson et al., 2002)	1.5μmNMRC (1)	15/20/30 40/50	30	200/1k/3k 9k/30k	26	-
(Gulinatti et al., 2005) (Ghioni et al., 2006)	CNR-IMM	20/50 100/200	24	300/700 4k/40k	38	30/30 31/35
(Rochas et al., 2002)	HV0.8μm (4)	80	19.5	-	-	-
(Rochas et al., 2003a) (Stapels et al., 2006)	HV 0.8μm (2)	7	25	900	30	60
(Zappa et al., 2004) (Zappa et al., 2005)	HV 0.8μm (2)	12	16	600	38	36
(Panchieri & Stoppa, 2007)	HV 0.7μm (2)	10x10 20x20 40x40	20.5 - 21	<10k <60k <200k	26	144
(Dandin et al., 2007)	0.5μm (5)	-	16.85	16k	-	-
(Mosconi et al., 2006)	HV 0.35μm (2 + IC)	20x20	28.3	3 – 5k	10	80
(Xiao et al., 2007)	HV 0.35μm (3)	-	45 - 50	<50	33	80
(Tisa et al., 2008)	HV 0.35μm (2 + IC)	20	24	<5k	37	39
(Niclass et al., 2006b) (Niclass et al., 2009)	0.35μm (2)	4/10	-	6/750	36	80
(Arbat et al., 2010a)	HV 0.35μm (2)	20x20	17.3	3.4k	-	-
(Finkelstein et al., 2006a) (Finkelstein et al., 2006b)	180nm IBM (6)	2x2 14x14	10	185k	12 - 20	-
(Faramarzpour et al., 2008)	180nm (2)	10/20	10.2	60k(10) 240k (20)	45	-
(Niclass et al., 2007a) (Niclass et al., 2007b)	130nm mod (2)	10	10	100k	41	144
(Gersbach et al., 2008) (Gersbach et al., 2009)	130nm mod (6)	4.3	10/17.2	1M/90k	36	125
(Richardson et al., 2009)	130nm STM (3)	8	14.4	<20	28	200
(Arbat et al., 2010b)	130nm STM (2)	20x20	10.5	3.5k	-	-
(Arbat et al., 2010b)	130nm STM (6)	20x20	10.55	1200k	-	-
(Karami et al., 2010)	90nm mod (2)	8x8	10	8.1k (0.13V)	8 - 14	398

Table 3. CMOS planar APDs. Termination (see section 2.3): 1-N+diffusion over p-well. 2-P-guard ring. 3-Deep p-well. 4-P-diffusion. 5-P-guard and polysilicon control gate. 6-Shallow trench isolation

technologies. Table 3 contains a summary of the published structures fabricated using planar technologies. See section 2-3 for details about termination. Some performances are associated to these devices, such as the possibility of integrating the electronics of the detector, of developing arrays of sensors, and of using low voltages and reducing the power consumption of the devices. One of the main disadvantages of the utilization of standard fabrication processes is the impossibility of modifying the fabrication process without the foundry interaction, inhibiting the possibility of device optimization.

2.3 Termination techniques for planar APDs

As commented before, the working principle of APDs requires a uniform electric field in the whole active area, what is only achieved in the central part of the sensor. Electrical-field concentration at the edges of the active area disturbs this uniformity and can cause premature edge breakdown, PEB. Different techniques have been developed in order to avoid PEB and consequently the device failure (Charbon, 2008), with the objective of limiting the electric field at the edges to be weaker than at the central multiplication region. Some of the most used options are summarized next.

Adding an n+ layer between the n substrate and the p surface confines the high electric field at the central part of the sensing area (Fig. 3), owing to the higher doping at the central junction (p-n+ instead of p-n at the edges). The concept was used with a p enrichment below the n+ diffusion to confine the electric field (Spinelli et al., 1998 and Jackson et al., 2000).

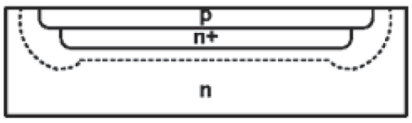

Fig. 3. N+ layer added between the n substrate and the p surface to avoid PEB. Termination technique (1) in table 3.

A second option largely used consists on the implementation of a p guard ring with lower doping level around the structure (Niclass et al., 2006b and Stoppa et al., 2005). This structure allows the possibility to share n-tubs between different sensors, reducing the pitch (Pancheri & Stoppa, 2007), and can be used in triple-well technologies which provide low-doping layers, as in the case of HV-CMOS (Xiao et al., 2007). This last approximation avoids heavily doped layers which are prone to have generation and trapping centres. Fig. 4 shows the initial and triple-well structures. Sensor arrays have been demonstrated with this technology (Tisa et al., 2008 and Arbat et al., 2010a) and it suitability has also been demonstrated in submicron technologies (Faramarzpour et al., 2008), but it is always important to avoid the full depletion of the n well, which would lead to punch through between the well and the substrate.

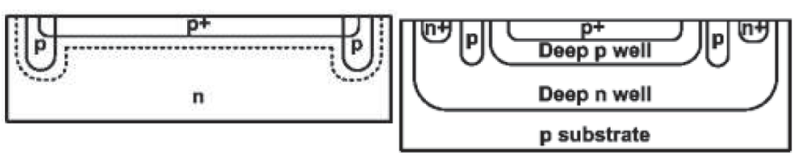

Fig. 4. Structures for avoiding PEB based on p-well guard ring at left, termination technique (2) in table 3, and deep tubs available in HV-CMOS technologies at right, termination (3) in table 3.

A third option frequently used consists on a p diffusion close to the edge of the p well at the sensing area (Rochas et al., 2002). In this case, the ion lateral diffusion during the processing generates a low-doped n region between p zones which can be completely depleted thanks to the biasing of an additional gate located on it (fig. 5, left). When using a p-substrate technology with doble well, it is possible to build similar guard-ring structures (fig. 5, right) with adjacent n wells placed at the minimum distance allowed by the technology (Dandin et al., 2007).

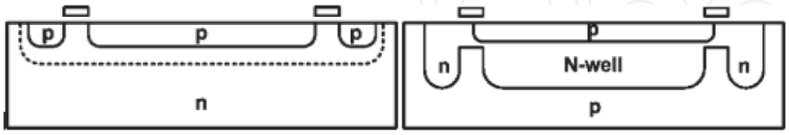

Fig. 5. Double low-doped n-well structure with gates (left) and guard rings and control gate signal (right). Termination techniques (4) and (5) in table 3, respectively.

Finally, for technologies beyond 250nm, the use of shallow trench isolation, STI, becomes a technological solution to reduce the negative effects of the birds-beak-shape of the SiO_2 (Finkelstein et al., 2006a). The STI prevents punch-through and latch-up, and it confines the electric field because the dielectric strength of SiO_2 is much higher than that of Si (fig. 6).

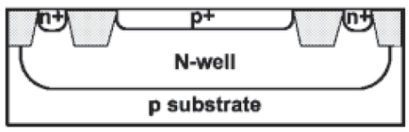

Fig. 6. Structure to avoid PEB based on STI elements. Termination technique (6) in table 3.

All these strategies have demonstrated suitability for preventing PEB, but not all of them are possible in a specific technology. The better choice depends on the possible structures.

3. G-APD simulation and characterization

Characterization of the individual sensing elements is needed for detector design, using different test benches and a black Faraday box. This section analyzes firstly the possibility of physical description of the device, to better understand its optical and electrical characteristics. Next, the characterization techniques usual for APDs are introduced: the I-V characteristic of the detector gives information about the breakdown voltage, the dark current below breakdown (linear mode) and the avalanche current. A 4-wire setup directly connected to the sensor terminals is recommended. Finally, the noise figures need to be characterized: dark count rate, afterpulsing and optical and electrical crosstalk. These parameters are not evident to minimize, and a definitive reading of actual detection requires new strategies based mainly on the accompanying electronics, as exposed in next section.

3.1 Physical simulation

Three main aspects have to be taken into account to calculate the electrical behaviour of the G-APDs: firstly, the charges generated in the semiconductor during the breakdown phenomenon; secondly, the movement of these charges inside the device towards its

electrodes; and thirdly, the influence of the external circuitry on the recorded signal after detection, which is the only result that can be compared with experimental data.

Interaction between radiation and matter is a statistical phenomenon that can be calculated via Monte Carlo models able to describe a particle or photon beam as it interacts with the different layers in a device. The conventional model that explains the generation-recombination processes via traps is the well known Shockley-Read-Hall model (Shockley & Read, 1952), in which four basic mechanisms are supposed to be involved: electrons and holes capture and electrons and holes escape from a trap. However, for high electric field, tunnelling effects are dominant, and newer models are introducing corrections to take them into account.

So long, Monte Carlo calculations have then allowed a detailed description of a beam inside a device, discriminating the contribution of tunnelling to the dark-count rate, and explaining most of the inner effects of absorption, backscattering, etc. referred to a given structure (Vilà et al., 2011). After that, the evolution of the generated charges must be described, and classical drift-diffusion models can give some macroscopic parameters related to interactions. However, the avalanche is difficult to be described via these semi-classical models, as the impact-ionization process itself depends at nearly atomic level on the generated fields, which in turn depend on the generated charge. In particular, the ionization coefficients for electrons and holes can be calculated for biasing up to the breakdown voltage, but for higher polarizations the charges generated by impact ionization modify locally the electric field, so that the coefficients get stabilized and no further progress can be calculated for any overvoltage. Solving this situation needs further advances in models.

Consequently, proprietary software needs to be developed and applied to properly describe the avalanche, and then, well established electrical models will help describing the device inside the whole detector system. The complete simulation process is complex, but necessary to understand the device behaviour in operating systems as for characterization.

3.2 I-V characteristics

The breakdown voltage is evidenced by a sudden current increase of several orders of magnitude in I-V characteristics for reverse bias. It is strongly technology dependent, because it is related to concentration and depth of the doping profiles, and can even be sensitive to the particular run and chip, as illustrated in fig. 7 (Arbat et al., 2010b). The analysis of the temperature effect on the breakdown voltage indicates that both parameters increase together. All these variations can be managed with adequate readout electronics.

3.3 Dark count rate

The dark-count rate increases exponentially with biasing, as shown in figure 8, and approximately linearly with the detector area. However, important differences can be found depending on the technology used. In particular, the trench-based structures present much more dark counts than the structure based on an n well. This suggests that the fabrication of these trenches introduces traps in their walls, increasing the pulse-generation probability (Hamamoto, 1991). Consequently, trench-based technologies should be treated with care when a low noise rate is required. The influence of other factors such as degradation due to radiation is still to be studied.

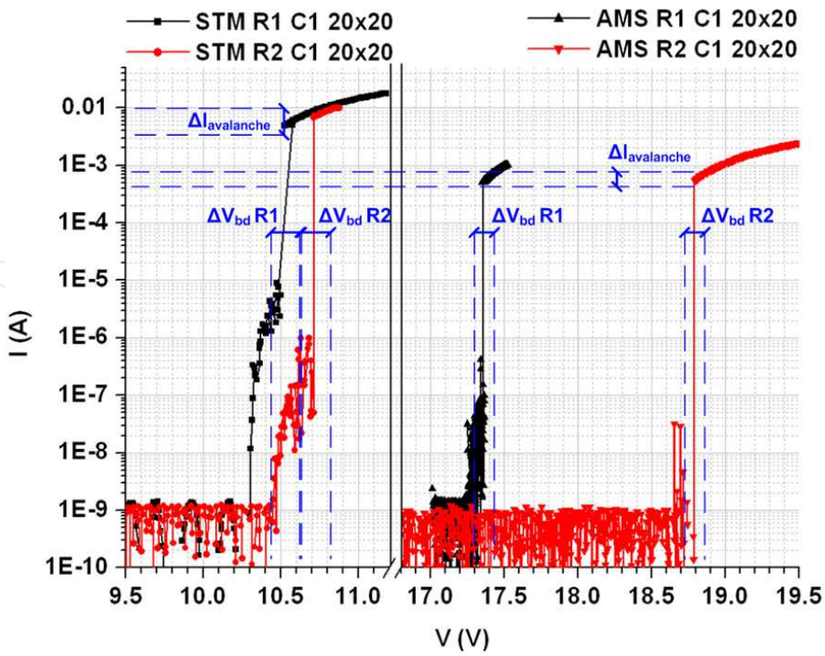

Fig. 7. I-V characteristics of 20µmx20µm APDs made using STM (left) and HV-AMS (right) technologies, for two different runs (R1 and R2) each.

An analysis with the temperature allows observing that the number of dark-count pulses increases exponentially with the temperature, as expected due to thermal generation of electron-hole pairs. The dynamic-range analysis of these types of structures gives sensibilities with similar behaviour independently from the technology, incrementing the counts linearly with illumination, until saturation is reached. On the other hand, increasing biasing raises the sensor sensibility.

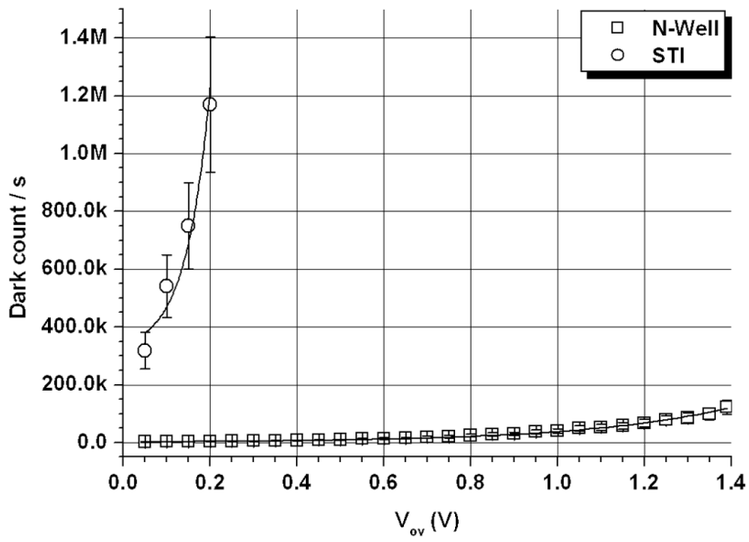

Fig. 8. Dark-count rate for two detector structures based on n-well and on shallow-trench isolation, STI, respectively, vs. operation voltage, V_{op}.

3.4 Time response and afterpulsing

Direct displaying of the voltage measurements vs. time indicates the afterpulsing behaviour of a sensor. Figure 9 shows the noise counts shortly after the pulse generation. Although the probes capacitance introduces some deformation of the signal, this type of graph also allows analyzing in some detail the time response of the sensor. For different technologies there are clear different timing behaviours, which can be summarized in a longer quenching time for n-well structures as compared to trench based ones, what favours the probability of charge trapping and increases afterpulsing. When the quenching and readout circuits are introduced into the ASIC, this quenching time can be reduced, as well as the probability of afterpulsing. Another noticeable remark is the longer dead time for n-well than for trench structures, which should be reduced by implanting active-recharge systems.

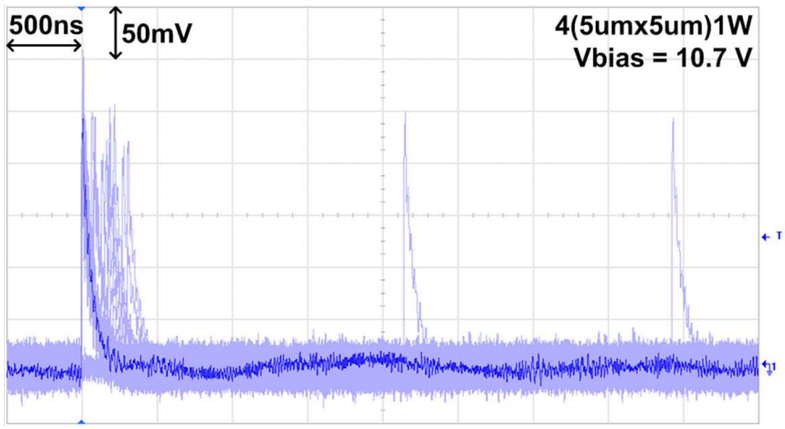

Fig. 9. Afterpulsing and noise visible in direct displaying vs. time.

3.5 Sensitive areas and cross-talk in APD arrays

A novel method has been recently reported to characterize APD-arrays response with high space resolution, whose results suggest that the fill factor can be drastically improved via good control of the doping profiles (Vilà et al., 2011). This research represents a novel effort to use APDs to construct an active pixel detector for charged particles in colliders. The key issue consist on using a focused ion beam/scanning electron microscopy, FIB/SEM setup to precisely characterize the sensitive areas and the quantum efficiency. The beams provided by FIB/SEM setup are nanometric, in contrast to usual test beams that lighten the detectors with lasers providing spots of several tens of microns -comparable to detector dimensions.

A FIB/SEM setup allows a beam to be accelerated, collimated into a nanometric spot and focused with nanometric precision onto one pixel, as well as to perform a detection experiment without trigger setup, thanks to the controlled amount of particles injected per measuring time. The beam is scanned from a pixel to its neighbour one, as shown in figure 10-left, and the agreement between the mathematical description of the detection events and the measurement corroborates both. The measured detection profiles are as shown in figure 10-right, where different applied bias are represented. The position and separation between adjacent pixels is marked onto the profiles taking onto account their distance on the layout, the width of the guard rings and their lateral diffusion.

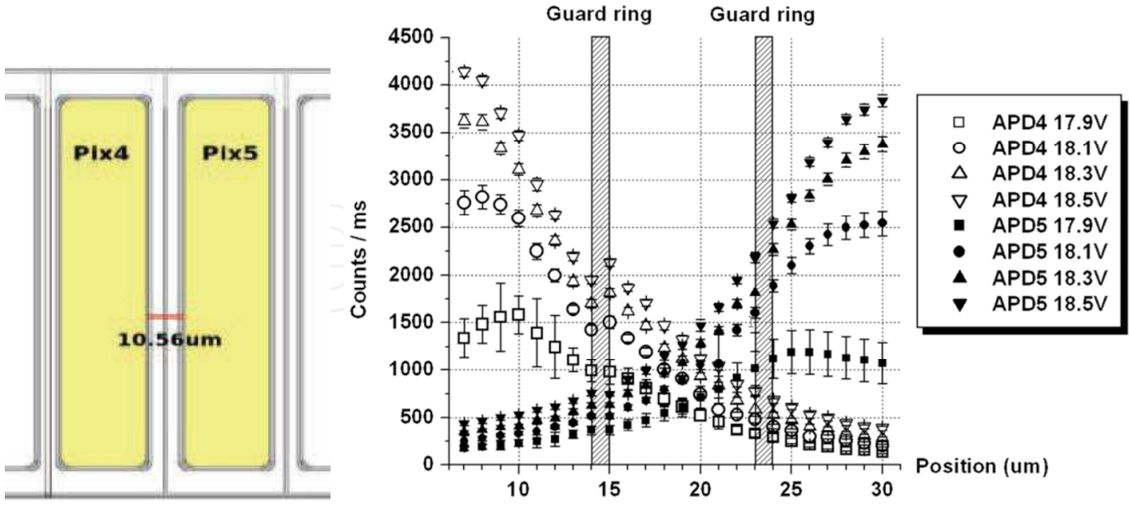

Fig. 10. Layout of the pixels used for sensitive-area and crosstalk demonstration (left). Detection frequencies measured by scanning a 30kV electron beam onto these two neighbouring pixels (right).

It is important to remark that this new characterization is only useful with a detailed functional simulation. The qualitative agreement between Monte Carlo calculations and experimental detection frequencies under a low-flow electron beam (Vilà et al., 2011) avails the correctness of both and suggests good efficiency for the APD prototypes. The nanometric dimension of the beam, as well as its accurate positioning onto the APD array, allows a detailed study of the dead areas around pixels, where the high detection rate observed suggests a noticeable efficiency of the guard ring as detector. This situation could improve drastically the fill factor of the devices, which could virtually arrive to 100%.

4. Circuitry involved in the G-APD operation

The improvement of the sensor performances has been strongly influenced by the development of the related electronics. In the case of dedicated technologies, the quenching electronics is implemented externally to the sensor. In the case of monolithic technologies, the quenching and any additional signal processing can be done close to the sensor, allowing an increase of functionality while reducing area, consumption and power requirements. In this section, basic circuits will be revised, starting from some SPICE models for describing the behaviour of the APDs.

4.1 Models for APD detectors

In order to develop a complete electronic system involving the sensor, an electrical model will be necessary for it. Few models are already available to reproduce partially the behaviour of the APD, but they do not offer a complete vision of the sensor. Recent developments are summarized in this section.

Since the initial investigations of the p-n junction characteristics, developed after the Shockley prediction (Shockley, 1961) and confirmed on the early '60s (Goetzberg et al., 1963), the multiplication behaviour of such structures working in Geiger mode generated a great expectation. The first electrical model was developed as a consequence of these studies (Haitz, 1965) and has been largely used. The model contemplates the parasitic capacitances of the device and reproduces the junction behaviour when a photon is detected. Recently, a second model was presented, using programmable voltage switches (Dalla Mora et al., 2007). In this model, a voltage programmable source is used to reproduce the different behaviours of the APD current depending on the bias. It also contemplates the self-sustaining process reached in APDs when the current rises to a certain threshold. An alternative to this model includes a voltage-controlled switch to reproduce both the static and dynamic behaviours (Mita et al., 2008). The switch is defined in Verilog-A language, and the model also deals with the dependence of the device capacitance on the reverse bias. A newer modification includes the current-voltge behaviour of a diode in the whole polarization range. It adds forward behaviour and the second breakdown (Zappa et al., 2009). The model is presented for both SPICE and Virtuoso Spectre simulators. All these three fundamental models are presented in figure 11.

However, all the models presented so far lack to consider uncorrelated (dark counts) and pulse-correlated (afterpulsing) noises. The electronics used after the sensor has to be designed considering that these false hits must be stored for postprocessing. The first model including diode behaviour for all the polarization range and noise reproduction has been presented recently (Arbat et al., 2010b). Its validity is demonstrated by adjusting the measurements obtained after the characterization of two different APD structures fabricated with a standard 130nm CMOS processing.

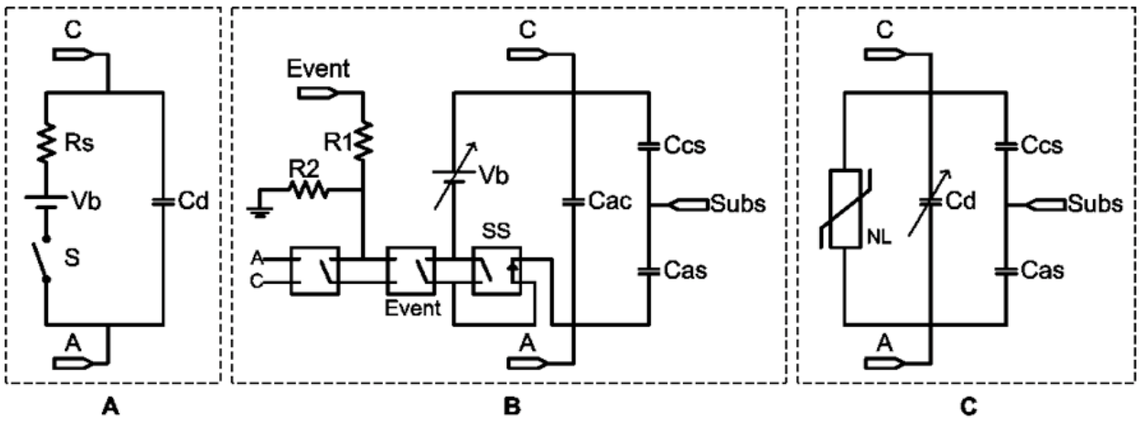

Fig. 11. Models for APDs operation: A) (Haitz et al., 1965), B) (Dalla Mora et al., 2007) and C) (Mita et al., 2008).

This new model uses a source with a noise pattern, together with other active and passive components from Spectre (Cadence™), to reproduce the noise behaviour in the time

domain. (Arbat, 2010b). The noise transitory analysis available from the Cadence™ software since version 2008 (Cadence, 2008) allows the possibility of reproducing the actual sensor behaviour. Including the noise behaviour in the model it is possible to obtain information about the probability of information losses due to the dead time related to the noise generation. It also allows studying the strategies that can be used for avoiding the noise interference into the signal, such as gated-mode acquisition or active quenching and recharge circuits. Finally, the analysis of architectures for array readout considering the generated noise, indistinguishable from the signal, is also possible.

The model is represented in figure 12. It contains the elements presented in the previous models, such as anode-cathode capacitor, C_{ac}, the anode-bulk capacitor, C_{ab}, and the cathode-bulk capacitor, C_{cb}. However, the different I-V regions are reproduced with three different groups of resistor, voltage source and voltage controlled switch. The first branch models the forward behaviour of the diode, V_f, allowing the current flow when the forward bias is higher than the bandgap. The second branch represents the second breakdown (Vb2) related to the breakdown of the lateral sensor junctions.

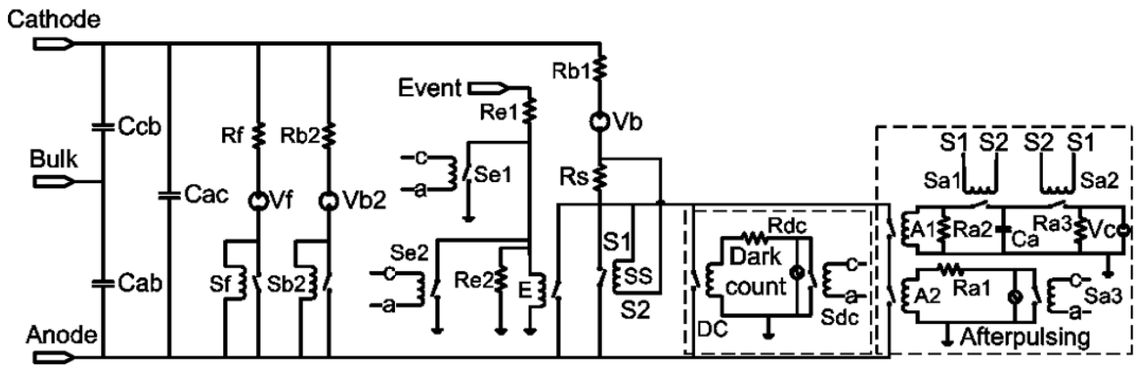

Fig. 12. APD model containing I-V behaviour and noise sources for dark counts and afterpulsing.

Finally, the third branch corresponds to the Geiger-mode region (V_b), and has been modified from the previous models to include noise effects. It offers four possible ways to allow conductivity between both terminals: photon/particle arrival (E), self-sustaining avalanche (SS), dark-count event (DC) and afterpulsing generation (A1-A2). To reproduce the spurious nature of dark-count pulses, the source of the model generates a random noise signal with the frequencies obtained during the sensor characterization. Similarly, to reproduce afterpulsing events, the sensing resistor Rs is used to sense the current flowing between anode and cathode during an avalanche.

The novelty of this model is to add these sources of noise to an electrical model of the sensor, and its validity has been tested by comparison with experimental measurements obtained after characterization of two APD structures fabricated with a standard 130nm CMOS process. Figures 13 A, B and C summarize the obtained results, demonstrating the validity of this newest model for APDs.

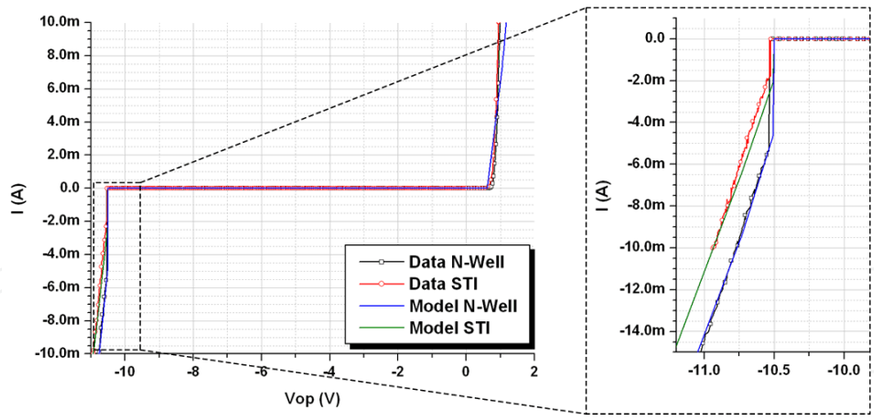

A

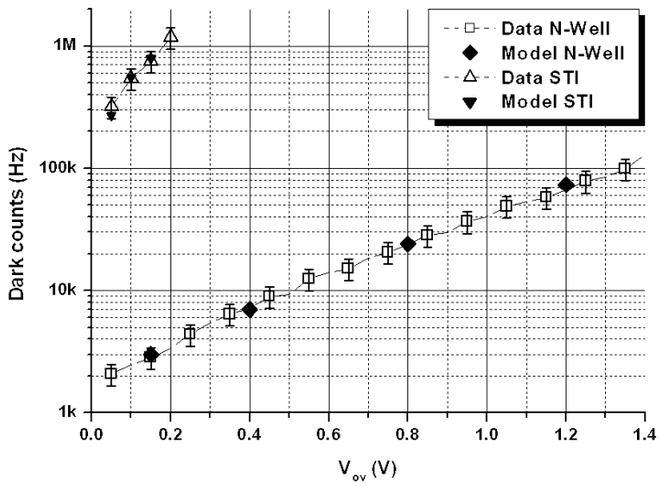

B

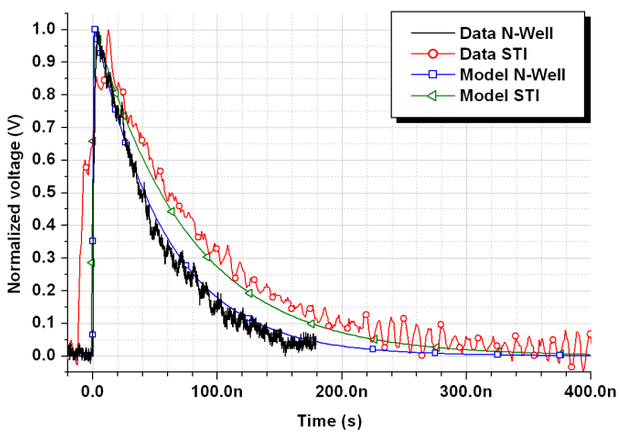

C

Fig. 13. A) I-V measurements and simulation using the models for an N-well and a STI structures. B) Dark counts measured for the N-well and the STI structures with a 10 kΩ quenching resistance. C) Time response of the two structures and the models represented with a normalized voltage and a quenching resistance of 10 kΩ.

4.2 Quenching and recharge circuits

The dead time, i.e. the total time between the start of a pulse and the resetting of the bias voltage after quenching and recharge, limits the device speed. Many different circuits have been developed to minimize this time, which can be divided into active, passive or combination of both. In all cases, the avalanche reading is done by converting analogue signal to digital by means of a comparator.

As the simplest approximation, a passive quenching circuit (Cova et al., 1996) can be obtained by connecting a high-valued quenching resistance, R_q, in series to the APD (fig. 14). As the avalanche current starts to flow, the resistance forces the operating voltage, V_{op}, to drop down to the breakdown voltage, V_{bd}, quenching the avalanche. This process is not instantaneous because of the parasitic capacitance of the diode, but follows an exponential decay determined by R_qC_{APD} and the avalanche current. Also the circuit recovery after quenching is exponential, but slower owing to the recharge current is much lower than the avalanche current. The sum of the quenching, T_q, and recharge, T_r, times corresponds to the dead time, T_{dead}, which in this case is quite long.

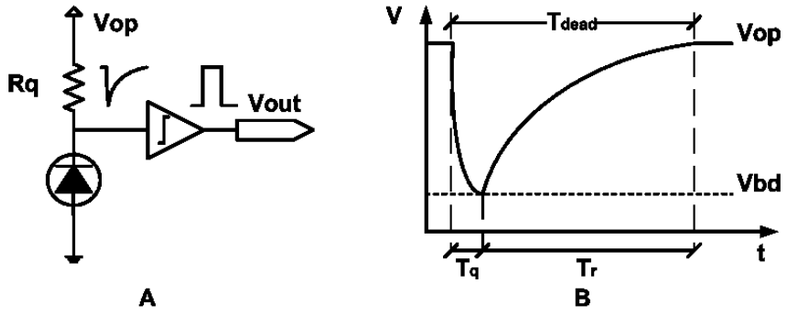

Fig. 14. A) Both passive quenching and recharge circuits. B) Sketch of the timing behaviour.

The next development of the passive quenching for integrated APDs corresponds to the use of a saturated MOS transistor as quenching resistance (figure 15). During the recharge period, the transistor works as a variable resistor, thanks to the change in the biasing.

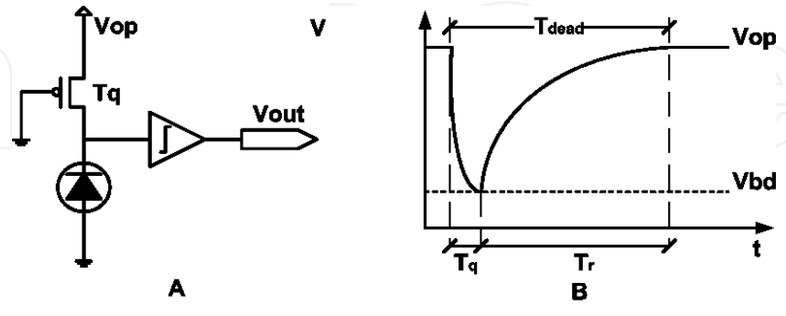

Fig. 15. A) Passive quenching by a transistor and detecting circuits. B) Sketch of the timing behaviour.

As the main contribution to the dead time is due to the recharge stage, a first improvement can be obtained by using active recharge. A simple circuit to provide it consists of an additional MOSFET with low capacitance as switch in parallel to the quenching resistor.

The circuit in figure 16 includes a 50Ω resistor R_s to match impedances with the measuring circuit. When the avalanche is detected, the comparator generates signal, the switch is closed and the sensor recovers the operating voltage, V_{op}. When the process is finished, the switch is opened again and the detector becomes ready for a new detection. This implementation reduces the dead time, but it can increase the afterpulsing noise, as the traps filled during the avalanche may not be released.

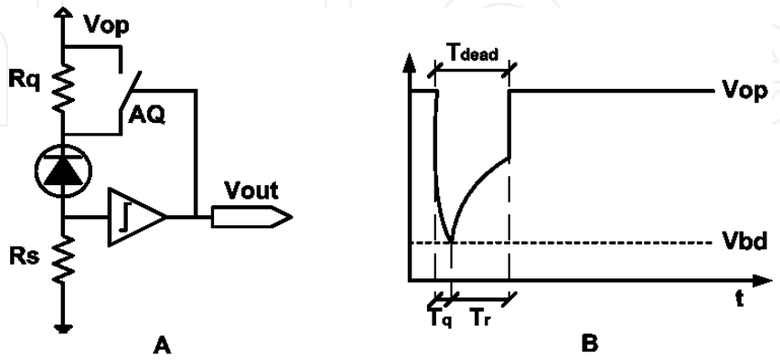

Fig. 16. A) Passive quenching and active recharge by a switch AQ. B) Sketch of the timing behaviour.

Using an active quenching can reduce afterpulsing noise, as the probability for a charge to be trapped is proportional to the duration of the avalanche event. A simple way to generate an active quench is to connect a switch between the APD and a voltage source below the breakdown (figure 17). When the avalanche is detected, the switch is closed and the sensor is quickly biased to this low voltage, producing fast avalanche quenching and limiting the charge through the detector.

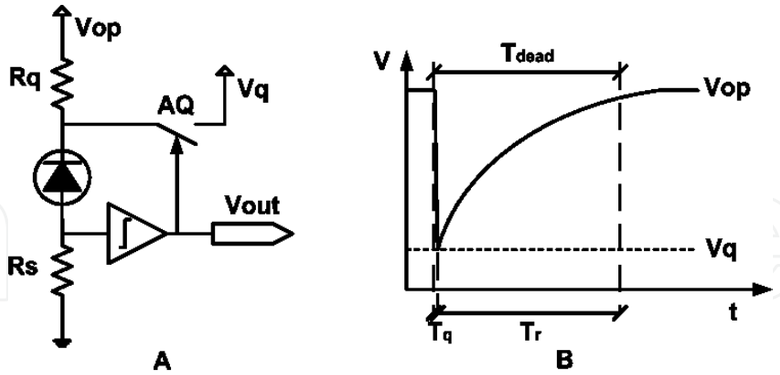

Fig. 17. A) Active quenching with passive recharge. B) Sketch of the timing behaviour.

The most complete approach to improve timing consists of both active quenching and recharge (figure 18). When an avalanche pulse is sensed, the comparator activates the voltage driver, which switches AQ and lowers the biasing down to the breakdown voltage. After a hold-off time (not represented in the figure), the bias voltage is switched back to the operating level by using AR. This circuit reduces the sensor dead time allowing to reach rates of million counts per second while maintaining the high resolution in photon timing.

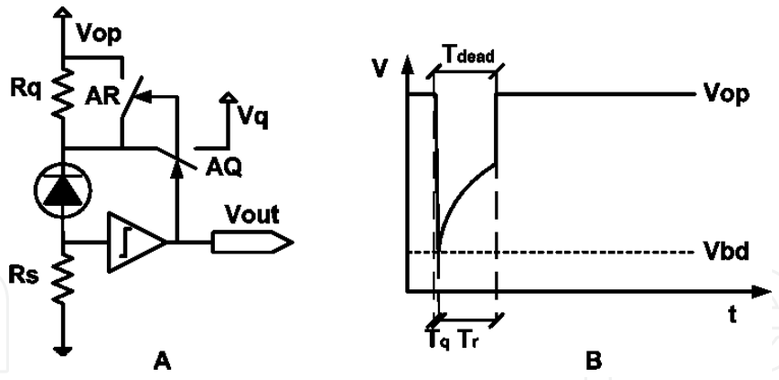

Fig. 18. A) Active quenching by switch AQ and recharge by switch AR. B) Sketch of the timing behaviour.

The development of improved active quenching and recharge circuits has been important. Integrated circuits including improvements of this simple approach have been reported (Zappa et al., 2000 and 2002) involving mixed passive-active circuit configurations that combined integrated circuit with external components (figure 19).

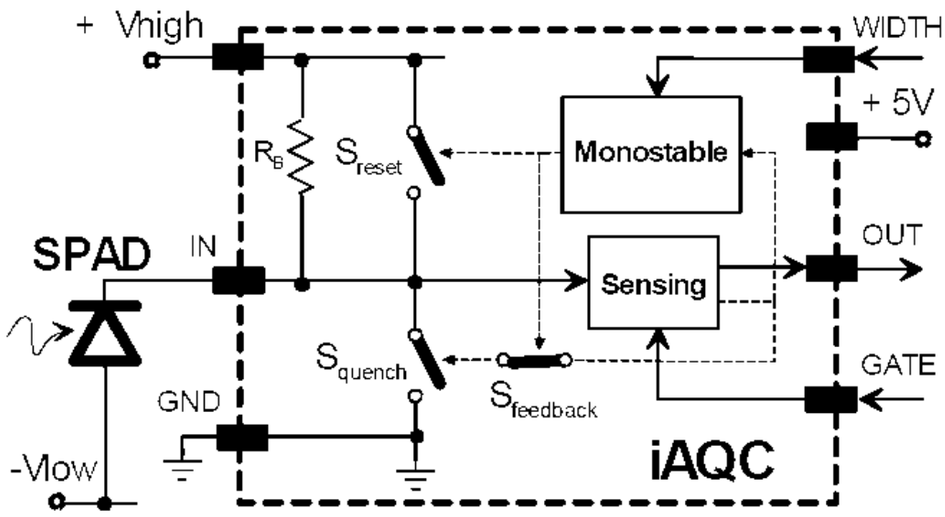

Fig. 19. Integrated active quenching and recharge structure (Zappa et al., 2002).

4.3 Operation modes and readout methods

APDs can be always reverse-biased at a fixed voltage above V_{BD}, so that they are always ready to detect (free running). However, in those applications where the signal arrival time is known, the sensor can also be activated only in certain periods (gated acquisition). In contrast with the free-running operation mode, in the gated acquisition mode the reverse bias voltage swings from over to under V_{BD} to periodically enable and disable the photodiode. In this way, the sensor is kept active only for short periods of time that can be synchronized with the expected signal arrival. Consequently, the probability to detect dark counts interfering with the signal-triggered ones is linearly reduced with the width of the active period of the sensor without missing any photon counts, and hence the signal/noise

ratio is improved (Vilella et al., 2011a and b). In addition, long enough non-active periods, longer than the lifetime of the trapping levels, allow to completely eliminate the afterpulsing probability. The basic circuits for running in gated mode can be seen in figure 20.

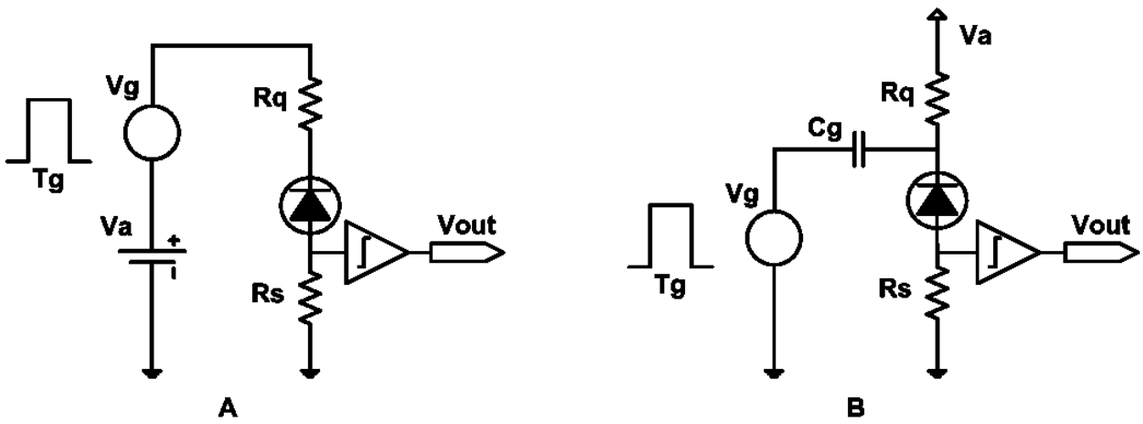

Fig. 20. Circuits for gated-mode operation. A) DC coupling and B) AC coupling.

Recently, a new prototype having the front-end electronics for gated acquisition monolithically integrated with the G-APD has been demonstrated (Vilella et al., 2011a and b). The pixel detector, based on a gated G-APD with passive quenching and active recharge (through RST transistor), is shown in figure 21. The operation mode, together with suitable readout electronics that allows low reverse overvoltage, reduces both the dark-count rate and probability, and eliminates afterpulsing at the pixel. Also, gating with shorter observation periods allows a considerable increase in the sensor dynamic range.

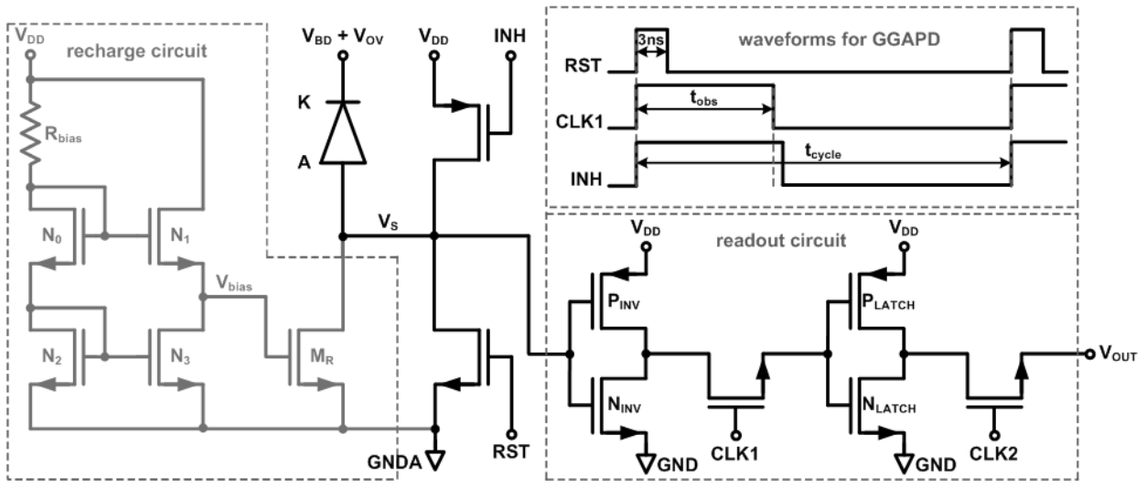

Fig. 21. Schematic diagram of the pixel detector integrated with gated-acquisition electronics, with the waveforms of the gated acquisition, in the inset up right (Vilella et al., 2011b).

Finally, several readout circuits for CMOS G-APDs allowing low-noise operation have been also reported (figure 22), to complete the previous sensor with gated acquisition (Vilella et al., 2010 and 2011b). By using a front-end circuit based on a floating ground, avalanche

detections were possible for very low overvoltage, which also reduced the dark-count rate. The characterization of this pixel showed that it could provide acceptable performance even for high-speed applications.

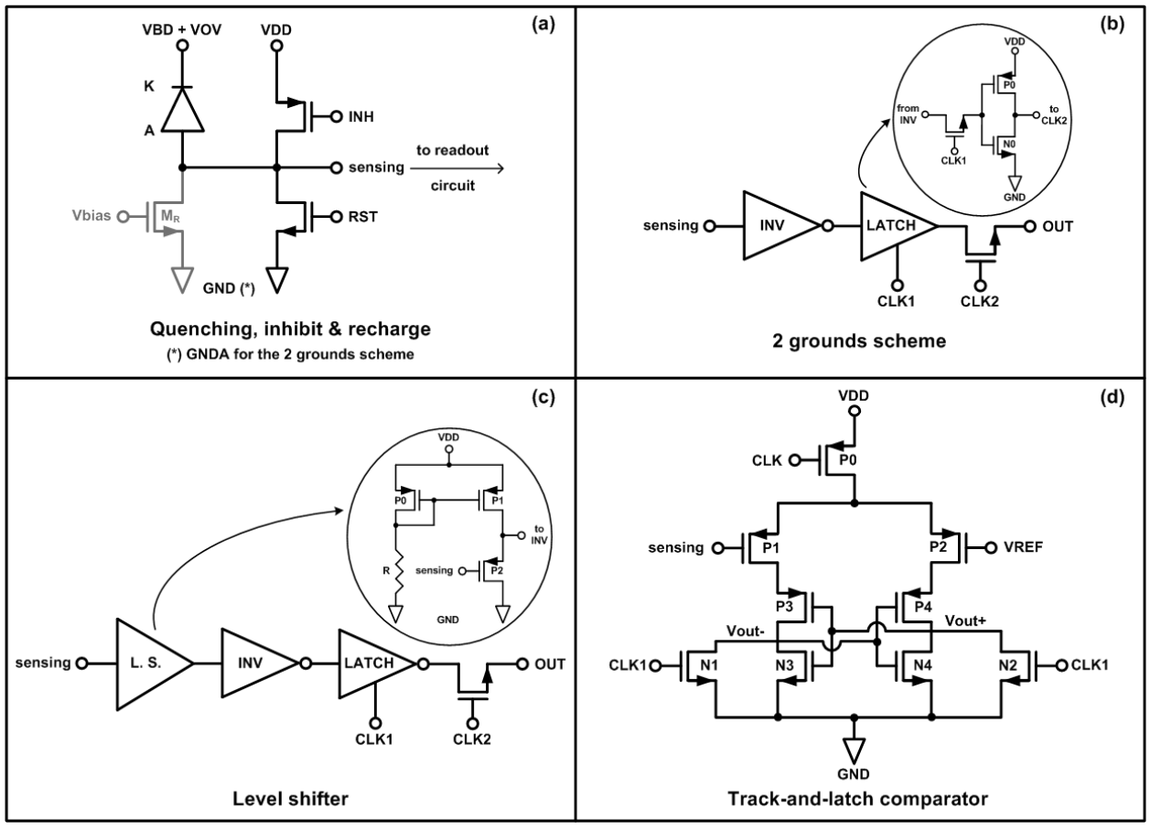

Fig. 22. A) Generic schematic diagram of the structure with gated acquisition. B) Readout circuit based on a 2-grounds scheme, C) on a level shifter and D) in a track-and-latch comparator (Vilella et al., 2011b).

4.4 Readout options for G-APDs arrays

Finally, G-APDs are usually used in large area applications that require their organization in sensor arrays or cameras. The reading options of a camera are mainly related to its final application: for imaging every pixel must be read, while for an even-driven information, such as the position of a particle arrival, only the information of the hit pixels is needed. Consequently, a detector array can be read sequentially, i.e. all the elements are read in an ordered way, or event-driven, what means reading only the pixels in which some signal has been detected. The sequential readout can also be performed with one or several output lines (figure 23 A and B), being possible to adjust the data-transfer speed to the application-required speed. In this case, every pixel contains the basic quenching and recharging circuits together with the elements for selecting row and column (Niclass & Charbon, 2005). On the contrary, in event-driven readout only the pixels that have received a pulse are read (figure 23 C), and this is optimal when only a small part of the array receives information. In this case, the electronics becomes more complicated than for sequential readout, but the timing is noticeably reduced (Niclass et al., 2006a).

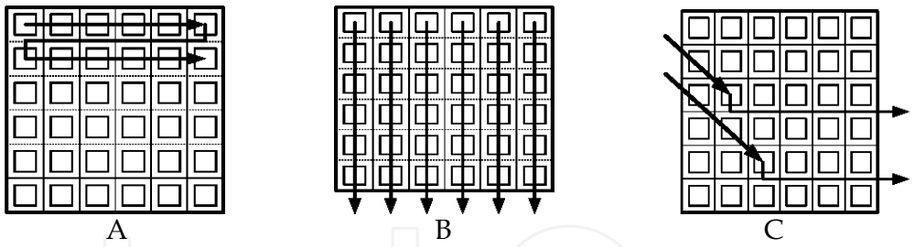

Fig. 23. Sequential readout for a detector array, with only one (A) or several (B) outputs. In C, event-driven readout mechanism.

After reading, signal must be processed, and, for some applications, the implementation of a part of this processing in the pixel can be very interesting (figure 24). In this case, the pixel-contained electronics becomes complicated, and readout of the whole camera after the complete measurement is required. A simplest circuit could be a pulse counter able to provide the image gray levels (Tisa et al., 2008 and 2009).

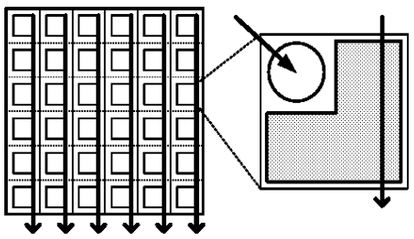

Fig. 24. Electronic processing inside the pixel.

5. Summary and conclusions

A general overview of the main aspects related to Geiger-mode avalanche photodiodes has been exposed in this chapter. Those sensors have been largely used for single photon detection, and nowadays are also used for X- and gamma-rays detection and high-energy particles. After the revision of the main concepts related to their operation, dedicated and standard technologies have been considered from the historical review of their respective evolution. The different aspects corresponding to the different types of sensors, the related circuits and the measurement and definition of the principal figures of merit of the sensors have been presented. Recent developments of the scientific community related to the use of G-APDs have also been exposed here.

6. Acknowledgment

This work has been partially supported by the Spanish projects “Desarrollo de nuevas tecnologías en aceleradores y detectores para los futuros colisionadores de física de partículas”, coded FPA2008-05979-C04-02 and “Desarrollo de nuevos detectores para los futuros colisionadores en Física de Partículas”, coded FPA2010-21549-C04-01.

7. References

Alexander, S.B. (1997). *Optical communication receiver design (SPIE tutorial texts in optical engineering Vol. TT22),* SPIE publications, IEE Telecommunications Series Vol. 37, ISBN 0-8194-2023-9, Bellingham WA

Arbat, A., Trenado, J., Gascon, D., Vilà, A., Comerma, A., Garrido, L. & Dieguez, A. (2010a). High voltage vs. high integration: a comparison between CMOS technologies for SPAD cameras. *Proc. of SPIE Optics and Photonics 2010*, Vol. 7780, pp. 77801G, ISSN 0277-786X, San Diego CA, August 2010

Arbat, A. (2010b). Towards a forward tracker detector based on Geiger mode avalanche photodiodes for future linear colliders. PhD dissertation, December 2010

Assefa, S., Xia, F. & Vlasov, Y.A. (2010). Reinventing germanium avalanche photodetector for nanophotonic on-chip optical interconnects. *Nature,* Vol. 464, (March 2010), pp. 80-85, ISSN 0028-0836

Cadence. (2008). Application notes on direct time-domain noise analysis using virtuoso spectre, version 1.0

Charbon, E. (2007). Will avalanche photodiode arrays ever reach 1 megapixel?. *Proc. 2007 International Image Sensor Workshop*, pp. 246-249, Ogunquit ME, 2007

Charbon, E. (2008). Towards large scale CMOS single-photon detector arrays for lab-on-chip applications. *Journal of Physics D: Applied Physics* Vol. 41, (2008), pp. 094010-1:9, ISSN 0022-3727

Cova, S., Ghioni, M., Lacaita, A., Samori, C. & Zappa, F. (1996). Avalanche Photodiodes and Quenching Circuits For Single-Photon Detection. *Applied Optics*, Vol. 35, No. 12 (April 1996), pp. 1956-1976, ISSN 1943-8206

Cova, S., Ghioni, M., Lotito, A., Rech, I. & Zappa, F. (2004). Evolution and prospects for single-photon avalanche diodes and quenching circuits. *Journal of Modern Optics*, Vol. 51, No. 9-10 (June-July 2004), pp. 1267-1288, ISSN 0950–0340

Dalla Mora, A., Tosi, A., Tisa, S. & Zappa, F. (2007). Single-Photon Avalanche Diode Model for Circuit Simulations. *IEEE Photonics Technology Letters*, Vol. 19, No. 23 (December 2007), pp. 1922-1924, ISSN 1041-1135

Dandin, M., Nelson, N., Saveliev, V., Ji, H., Abshire, P. & Weinberg, I. (2007). Single photon avalanche detectors in standard CMOS. *IEEE Sensors '07*, ISSN 1930-0395, pp. 585-588, Atlanta, October 2007

Dautet, H., Deschamps, P., Dion, B., MacGregor, A.D., MacSween, D., McIntyre, R.J., Trottier, C. & Webb, P.P. (1993). Photon counting techniques with silicon avalanche photodiodes. *Appl. Opt.*, Vol. 32, No. 21 (1993), pp. 3894-3900, ISSN 2155-3165

Dussault, D. & Hoess, P. (2004). Noise Performance Comparison of ICCD with CCD and EMCCD Cameras, *Proceedings of SPIE*, Vol. 5563, pp. 195-204, ISBN 0-8194-5501-6, Denver, August 2004

EG&G (1996) Canada, Vaudreuil, P.Q., Canada, SPCM-AQ Series Data Sheet ED-0043/11/96, 1996

Faramarzpour, N., Deen, M.J., Shirani, S. & Fang, Q. (2008). Fully integrated single-photon avalanche diode detector in standard CMOS 0.18 µm technology. *IEEE Transactions on electron devices*, Vol. 55, No. 3 (March 2008), pp. 760-767, ISSN 0018-9383

Finkelstein, H., Hsu, M.J. & Esener, S.C. (2006a). STI-Bounded single-photon avalanche diode in a deep-submicrometer CMOS technology. *IEEE Electron Device Letters*, Vol. 27, No. 11 (November 2006), pp. 887-889, ISSN 0741-3106

Finkelstein, H., Hsu, M.J. & Esener, S. (2006b). An ultrafast Geiger-mode single photon avalanche diode in 0.18µm CMOS technology. *Advanced photon counting techniques, Proc. of SPIE*, Vol. 6372, ISBN 9780819464705, pp. 63720W-1:10, Boston MA, October 2006

Gersbach, M., Niclass, C., Charbon, E., Richardson, J., Henderson, R. & GRANT, L. (2008). A single photon detector implemented in a 130 nm CMOS imaging process. *Proc. of the 38th European Solid-State Device Research Conference, ESDERC 2008*, pp. 270-273, ISSN 1930-8876, Edinburgh, September 2008

Gersbach, M., Richardson, J., Mazaleyrat, E., Hardillier, S., Niclass, C., Henderson, R., Grant, L. & Charbon, E. (2009). A low-noise single-photon detector implemented in a 130 nm CMOS imaging process. *Solid-State Electronics,* Vol. 53, (May 2009), pp 803-808, ISSN 0038-1101

Ghioni, M., Cova, S., Lacaita, A. & Ripamonti, G. (1988). New silicon epitaxial avalanche diode for single-photon timing at room temperature, *Electron. Lett.*, Vol. 24, No. 24 (Nov. 1988), pp 1476-1477, ISSN 0013-5194

Ghioni, M. & Ripamonti, G. (1991). Improving the performance of commercially available Geiger-mode avalanche photodiodes. *Rev. Sci. Instrum.*, Vol. 62, No. 1 (January 1991), pp. 163-167, ISSN 0034-6748

Ghioni, M., Gulinatti, A., Rech, I. & Cova, S. (2006). Recent advances in silicon single photon avalanche diodes and their applications. *Annual Meeting of the IEEE Lasers and Electro-Optics Society, LEOS 2006*, ISBN 0-7803-9555-7, pp. 719-720, Montreal, October 2006

Ghioni, M., Gulinatti, A., Rech, I., Zappa, F. & Cova, S. (2007). Progress in silicon single-photon avalanche diodes. *IEEE Journal of selected topics in quantum electronics*, Vol. 13, No. 4 (July-August 2007), pp. 852-862, ISSN 1077-260X

Goetzberg, A., McDonald, B., Haitz, R. & Scarlett, R. (1963). Avalanche effects in silicon p-n junctions. II. Structurally perfect junctions. *Journal of App. Phys.*, Vol. 34, (1963), pp. 1591-1600 ISSN 0021-8979

Graugés, E., Comerma, A., Garrido, L., Gascón, D., Trenado, J., Diéguez, A., Vilà, A., Arbat, A., Freixas, L., Hidalgo, S., Fernández, P., Flores, D. & Lozano, M. (2010). Study of Geiger avalanche Photo-diodes (Galds) applications to pixel Trucking detectors. *Nucl. Inst. Met. Phys. Res. A,* Vol. 617, (2010), pp. 541-542, ISSN 0168-9002

Guerrieri, F., Tisa, S. & Zappa, F. (2009). Fast Single-Photon imager acquires 1024 pixels at 100 kframe/s. *Proceedings of SPIE*, Vol. 7249, pp. 72490U-1 – 72490U-11, ISSN 0277-786X, San José CA, January 2009

Gulinatti, A., Maccagnani, P., Rech, I., Ghioni, M. & Cova, S. (2005). 35 ps time resolution at room temperature with large area single photon avalanche diodes. *Electronic letters*, Vol. 41, No. 5 (March 2005), pp. 272-274, ISSN 0013-5194

Haitz, R. (1964). Model for the electrical behavior of a microplasma. J. Appl. Phys., Vol. 35, (1964), pp. 1370-1376 ISSN 0021-8979

Haitz, R. (1965). Mechanisms contributing to the noise pulse rate of avalanche diodes. J. Appl. Phys., Vol. 36, (1965), pp. 3123-3131, ISSN 0021-8979

Hamamoto, T. (1991). Sidewall damage in a silicon substrate caused by trench etching. *Applied physics letters*, Vol. 58, No. 25 (June 1991), pp. 2942-2944, ISSN 0003-6951

Jackson, J.C., Morrison, A.P. & Lane, B. (2000). Characterization of large area SPAD detectors operated in avalanche photodiode mode. *IEEE 13th Annual Meeting Laser and Electro-Optics Society, LEOS 2000*, Vol. 1, pp. 17-18, ISBN 0-7803-5947-X, Rio Grande, November 2000

Jackson, J.C., Morrison, A.P., Hurley, P., Harrell, W.R., Damjanovic, D., Lane, B. & Mathewson, A. (2001). Process monitoring and defect characterization of single photon avalanche diodes. *Proc. of the 2001 International Conference on Microeletronic Test Structures,* Vol. 14, pp. 165-170, ISBN 0-7803-6511-9, Kobe, March 2001

Jackson, J.C., Morrison, A.P., Phelan, D. & Mathewson, A, (2002). A novel silicon Geiger-mode avalanche photodiode. *Digest. International Electron Devices Meeting, IEDM'02,* ISBN 0-7803-7462-2, pp. 797-800, San Francisco CA, December 2002

Karami, M.A., Gersbach, M., Yoon, H.J. & Charbon, E. (2010). A new single-photon avalanche diode in 90nm standard CMOS technology. *Optics Express*, Vol. 18, No. 21 (October 2010), pp. 22158-22166, ISSN 0146-9592

Kindt, W.J. (1994). A novel avalanche photodiode array. *Nuclear Science Symposium and Medical Imaging Conference*, 1994 IEEE Conference Record, Vol. 1, (Oct-Nov 1994), pp. 164-167 ISBN 0-7803-2544-3, Norfolk, VA, Oct-Nov 1994

Lacaita, A., Cova, S. & Ghioni, M. (1988). Four-hundred-picosecond single-photon timing with commercially available avalanche photodiodes. *Rev. Sci. Instrum.*, Vol. 59, no. 7 (July 1988), pp. 1115-1121, ISSN 0034-6748

Lacaita, A., Ghioni, M. & Cova, S. (1989) Double epitaxy improves single-photon avalanche diode performance. *Electron. Lett.*, Vol. 25, No. 13 (June 1989), pp. 841-843, ISSN 0013-5194

Lacaita, A.L., Zappa, F., Bibliardi, S. & Manfredi, M. (1993). On the bremsstrahlung origin of hot-carrier-induced photons in silicon devices. *IEEE Transactions on Electron Devices*, Vol. 40, No. 3 (March 1993), pp. 577-582, ISSN 0018-9383

McIntyre, R. (1972). The distribution of gains in uniformly multiplying avalanche photodiodes: Theory, *IEEE trans. Electron Devices*, Vol. 19, No. 6 (June 1972), pp 703-713, ISSN 0018-9383

McIntyre, R. (1990). Silicon avalanche photodiode with low multiplication noise. *US patent* nº 4,972,242"

McIntyre, R. & Webb, P. (1996). Low-noise, reach-through, avalanche photodiodes. *US Patent* nº 5,583,352"

McKay, K.G. (1954). Avalanche breakdown in silicon. *Phys. Rev.,* Vol. 94, No. 4 (1954), pp. 877–884, ISSN 1943-2879

Mita, R., Palumbo G. & Fallica, P.G. (2008). Accurate model for single-photon avalanche diodes. *IET circuits devices systems*, Vol. 2, No. 2 (April 2008), pp. 207–212, ISSN 1751-858X

Mosconi, D., Stoppa, D., Pancheri, L., Gonzo, L. & Simoni, A. (2006). CMOS single-photon avalanche diode array for time-resolved fluorescence detection. *Proc. of the 32nd European Solid-State Circuits Conference, ESSCIRC'06*, ISSN 1930-8833, pp. 564-567, Montreux, September 2006

Niclass, C. & Charbon, E. (2005). A single photon detector array with 64x64 resolution and millimetric depth accuracy for 3D imaging. *IEEE International Solid-State Circuits Conference, ISSCC 2005*, pp. 364-366, ISSN 0193-6530, San Francisco, February 2005

Niclass, C., Sergio, M. & Charbon, E. (2006a). A CMOS 64x48 single photon avalanche diode array with event-driven readout. *Proc. of the 32th European SolidState Circuits Conference, SSCIRC'06,* pp. 556-559, ISBN 1-4244-0303-4, Montreux, September 2006

Niclass, C., Sergio, M. & Charbon, E. (2006b). A single photon avalanche diode array fabricated in 0.35µm CMOS and based on an event-driven readout for TCSPC experiments. *Proc. of SPIE, Advanced Photon Counting Techniques*, Vol. 6372, ISBN 9780819464705, pp. 63720S-1:12, Boston MA, October 2006

Niclass, C., Gersbach, M., Henderson, R., Grant, L. & Charbon, E. (2007a). A single photon avalanche diode implemented in 130 nm CMOS technology, *IEEE Journal of selected topics in quantum electronics*, Vol. 13, No. 4 (July/August 2007), pp. 863-869, ISSN 1077-260X

Niclass, N., Gersbach, M., Henderson, R.K., Grant, L. & Charbon, E. (2007b). A 130 nm CMOS single photon avalanche diode. *Proceedings of SPIE*, Vol. 6766 (2007), pp. 676606, ISSN 0277-786X, Boston, September 2007

Niclass, C., Favi, C., Kluter, T., Monnier, F. & Charbon, E. (2009). Single-photon synchronous detection. *IEEE Journal of Solid-State Circuits*, Vol. 44, No. 7 (July 2009), pp. 1977-1989, ISSN 0018-9200

Pancheri, L. & Stoppa, D. (2007). Low-noise CMOS single-photon avalanche diodes with 32 ns dead time. *37th European Solid State Device Research Conference, ESSDERC 2007,* ISSN 1930-8876, pp. 362-365, Munich, September 2007

Renker, D. (2004). Photosensors. *Nucl. Inst. and Meth. in Phys. Res. A,* Vol. 527, No. 1-2, (July 2004), pp. 15-20, ISSN 0168-9002

Richardson, J.A., Grant, L.A. & Henderson, R.K. (2009). Low dark count single-photon avalanche diode structure compatible with standard nanometer scale CMOS technology. *IEEE Photonics Technology Letters*, Vol. 21, No. 14 (July 2009), pp. 1020-1022, ISSN 1041-1135

Rochas, A., Pauchard, A.R., Besse, P.A., Pantic, D., Prijic, Z. & Popovic, R.S. (2002). Low-Noise silicon avalanche photodiodes fabricated in conventional CMOS technologies. *IEEE Transactions on Electron Devices*, Vol. 49, No. 3 (March 2002), pp. 387-394, ISSN 0018-9383

Rochas, A., Gani, M., Furrer, B., Besse, P.A., Popovic, R.S., Riborby, G. & Gisin, N. (2003a). Single photon detector fabricated in a complementary metal-oxide-semiconductor high-voltage technology. *Rev. Sci. Instrum.*, Vol. 74, No. 7 (July 2003), pp. 3263-3270, ISSN 0034-6748

Rochas, A., Gösch, M., Serov, A., Besse, P.A., Popovic, R.S., Lasser, T. & Rigler, R. (2003b). First Fully Integrated 2-D Array of Single-Photon Detectors in Standard CMOS Technology. *IEEE Photonics Technology Letter*s, Vol. 15, No. 7 (July 2003), pp. 963-965, ISSN 1041-1135

Sergio, M., Niclass, C. & Charbon, E. (2007). A 128x2 CMOS single-photon streak camera with timing-preserving latchless pipeline readout. *IEEE International Solid-State Circuits Conference, ISSCC 2007*, pp. 394-396, ISSN 0193-6530, San Francisco, February 2007

Shockley, W. & Read, W.T. (1952). Statistics of the recombinations of holes and electrons. *Phys. Rev.,* Vol. 87, No. 5 (September 1952), pp. 835-842

Shockley, W. (1961). Problems related to p-n junctions in silicon. *Solid-State Electron*. Vol. 2, No. 1 (January 1961), pp. 35-60, ISSN 0038-1101

Spinelli, A., Davis, L.M. & Dautet, H. (1996). Actively quenched single photon avalanche diode for high repetition rate time-gated photon counting. *Rev. Sci. Instrum.*, Vol. 67, No. 1 (January 1996), pp. 55-61, ISSN 0034-6748

Spinelli, A., Ghioni, M.A., Cova, S.D. & Davis, L.M. (1998). Avalanche detector with ultraclean response for time-resolved photon counting. *IEEE Journal of Quantum Electronics*, Vol. 34, No. 5 (May 1998), pp. 817-821, ISSN 0018-9197

Stapels, C.J., Lawrence, W.G., Augustine, F.L. & Christian, J.F. (2006). Characterization of a CMOS Geiger photodiode pixel. *IEEE Transactions on electron devices*, Vol. 53, No. 4 (April 2006), pp. 631-635, ISSN 0018-9383

Stapels, C.J., Squillante, M.R., Lawrence, W.G., Augustin, F.L. & Christian, J.F. (2007). CMOS-based avalanche photodiodes for direct particle detection. *Nucl. Inst. and Meth. In Phys. Res. A,* Vol. 579, No. 1 (2007), pp. 94-98, ISSN 0168-9002

Stoppa, D., Pancheri, L., Scandiuzzo, M., Simoni, A., Viarani, L. & Dalla Betta, G.F. (2005). A CMOS sensor based on signle photon avalanche diode for distance measurement applications. *Proc. of the IEEE. Instrumentation and measurement technology conference*, Vol. 2, ISBN 0-7803-8879-8, pp. 1162-1165, Ottawa, May 2005

Stoppa, D., Pancheri, L., Scandiuzzo, M., Gonzo, L., Dalla Betta, G.F. & Simoni, A. (2007). A CMOS 3-D imager based on single photon avalanche diode. *IEEE Transactions on Circuits and Systems - I*, Vol. 54, No. 1 (January 2007), pp. 4–12, ISSN 1057-7122

Tisa, S., Guerrieri, F. & Zappa, F. (2008). Variable-load quenching circuit for single-photon avalanche diodes. *Optics express*, Vol. 16, No. 3 (February 2008), pp. 2232-2244, ISSN 0146-9592

Tisa, S., Guerrieri, F. & Zappa, F. (2009). Monolithic array of 32 SPAD pixel for single-photon imaging at high frame rates. (2009). *Nucl. Instr. Meth. Phys. Res. A:*

Accelerators, Spectrometers, Detectors and Associated Equipment, Vol. 610, No. 1 (October 2009), pp. 24-27, ISSN 0168-9002

Vilà, A., Trenado, J., Arbat, A., Comerma, A., Gascon, D., Garrido, Ll. & Dieguez, A. (2011). Characterization and simulation of avalanche photodiodes for next-generation colliders. *Sensors and Actuators A: Physical,* (2011) doi:10.1016/j.sna.2011.05.011

Vilella, E., Arbat, A., Comerma, A., Trenado, J., Alonso, O., Gascon, D., Vilà, A., Garrido, L & Dieguez, A. (2010). Readout electronics for low dark count pixel detectors based on Geiger mode avalanche photodiodes fabricated in conventional CMOS Technologies for future linear colliders. *Nucl. Instr. Meth. Phys. Res. A*, Vol. 650, (2010), pp. 120-124, ISSN 0168-9002

Vilella, E., Comerma, A., Alonso, O. & Dieguez, A. (2011a). Low-noise pixel detectors based on gated Geiger mode avalanche photodiodes. *Electronics Letters*, Vol. 47, No. 6 (March 2011), ISSN 0013-5194

Vilella E., Arbat, A., Comerma, A., Trenado, J., Alonso, O., Gascon, D., Vilà, A., Garrido, L. & Dieguez, A. (2011b). Readout electronics for low dark count Geiger mode avalanche photodiodes fabricated in conventional HV-CMOS technologies for future linear colliders. *Topical Workshop on Electronics for Particle Physics 2010,* pp. C01015, Aachen, September 2011

Webb, P., McIntyre, R. & Conradi, J. (1974). Properties of avalanche photodiodes. *RCA Rev.*, Vol. 35, (June 1974), pp. 234-278, ISSN 0033-6831

Xiao, Z., Pantic, D. & Popovic, R.S. (2007). A new single photon avalanche diode in CMOS high-voltage technology. *International solid-state sensors, actuators and microsystems conference, Transducers 2007*, ISBN 1-4244-0842-3, pp. 1365-1368, Lyon, June 2007

Zappa, F., Ghioni, M., Cova, S., Varisco, L., Sinnis, B., Morrison, A. & Mathewson, A. (1997). Integrated array of avalanche photodiodes for single-photon counting. *Proc. 27th Eur. Solid-State Device Research Conf.*, pp. 600-603, ISBN 2-86332-221-4, Stuttgart, September 1997

Zappa, F., Ghioni, M., Cova, S., Samori, C. & Giudice, A. (2000). An integrated active quenching circuit for single-photon avalanche diodes. *IEEE Transactions on instrumentation and measurement*, Vol. 49, No. 6 (December 2000), pp. 1167-1175, ISSN 0018-9456

Zappa, F., Giudice, A., Ghioni, M. & Cova, S. (2002). Fully-Integrated Active-Quenching Circuit for Single-Photon Detection. *Proceedings of the 28th European Solid State Circuit Conference – ESSCIRC'02*, ISBN 88-900847-9-0, pp. 355-358, Firenze, September 2002

Zappa, F., Tisa, S., Gulinatti, A., Gallivanoni, A. & Cova, S. (2004). Monolithic CMOS detector module for photon counting and picosecond timing. *Proc. of the 34th European Solid-State Device Research Conference, ESSDERC*, ISBN 0-7803-8478, pp. 341-344, Leuven, November 2004

Zappa, F., Tisa, S., Gulinatti, A., Gallivanoni, A. & Cova, S. (2005). Complete single-photon counting and timing module in a microchip. *Optics Letters*, Vol. 30, No. 11 (June 2005), pp. 1327-1329, ISSN 0146-9592

Zappa, Z., Tosi, A., Dalla Mora A. & Tisa, S. (2009). SPICE modeling of single-photon avalanche diodes. *Sensors and Actuators A*, Vol 153, No. 2 (August 2009), pp. 197-204, ISSN 0924-4247

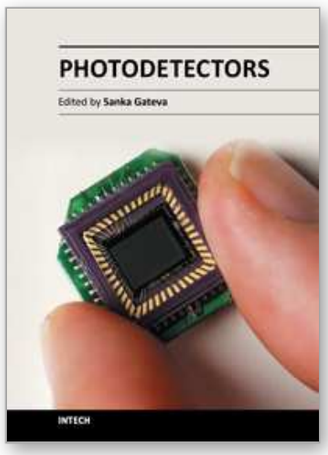

Photodetectors

Edited by Dr. Sanka Gateva

ISBN 978-953-51-0358-5
Hard cover, 460 pages
Publisher InTech
Published online 23, March, 2012
Published in print edition March, 2012

In this book some recent advances in development of photodetectors and photodetection systems for specific applications are included. In the first section of the book nine different types of photodetectors and their characteristics are presented. Next, some theoretical aspects and simulations are discussed. The last eight chapters are devoted to the development of photodetection systems for imaging, particle size analysis, transfers of time, measurement of vibrations, magnetic field, polarization of light, and particle energy. The book is addressed to students, engineers, and researchers working in the field of photonics and advanced technologies.

How to reference

In order to correctly reference this scholarly work, feel free to copy and paste the following:

Anna Vilà, Anna Arbat, Eva Vilella and Angel Dieguez (2012). Geiger-Mode Avalanche Photodiodes in Standard CMOS Technologies, Photodetectors, Dr. Sanka Gateva (Ed.), ISBN: 978-953-51-0358-5, InTech, Available from: http://www.intechopen.com/books/photodetectors/geiger-mode-avalanche-photodiodes-in-standard-cmos-technology

INTECH
open science | open minds

InTech Europe
University Campus STeP Ri
Slavka Krautzeka 83/A
51000 Rijeka, Croatia
Phone: +385 (51) 770 447
Fax: +385 (51) 686 166
www.intechopen.com

InTech China
Unit 405, Office Block, Hotel Equatorial Shanghai
No.65, Yan An Road (West), Shanghai, 200040, China
中国上海市延安西路65号上海国际贵都大饭店办公楼405单元
Phone: +86-21-62489820
Fax: +86-21-62489821

IntechOpen